JOURNAL OF CATALYSIS 126, 173–186 (1990)

Studies of Pt–Sn/Al_2O_3 Catalysts Prepared by Pt and Sn Coevaporation (Solvated Metal Atom Dispersion)

YONG-XI LI AND KENNETH J. KLABUNDE

Department of Chemistry, Kansas State University, Manhattan, Kansas 66506

Received September 25, 1989; revised June 11, 1990

Metal atoms of Pt and Sn have been solvated at low temperatures, and these solvated metal atoms have been used for depositing Pt–Sn bimetallic particles on Al_2O_3 (full SMAD method). Spectroscopic investigations with XPS, XRD, EXAFS, and Mössbauer have confirmed the presence of very small and/or amorphous Pt–Sn particles. Catalytic performance tests show that these particles are active for dehydrocyclization reactions, but depress unwanted hydrogenolysis reactions. Our results, compared with results for conventionally prepared and half-SMAD methods (Sn^0 on preformed Pt particles), show that Sn^0 within and on Pt particles has a significant effect on catalyst performance, and suggest that such performance can be predictably modified by using the correct preparation procedure (SMAD or conventional). The effect of tin is also perhaps now better understood due to these results.

INTRODUCTION

The solvated metal atom dispersion (SMAD) method allows the use of low-temperature solvated atoms as transient organometallic reagents for the deposition of atoms onto catalyst supports (*1, 2*). By continued deposition small metal clusters grow on the support surface, and these metal particles possess unusual catalytic properties that are due to surfaces free of oxides and unusual morphologies (*3*).

We have reported earlier on the preparation of Pt–Sn/SiO_2 and Pt–Sn/Al_2O_3 catalysts where tin was evaporated, solvated, and allowed to deposit on conventionally prepared supported platinum particles (the "half SMAD" method) (*4, 5*). In this way catalysts were obtained in which tin in the zero valent state was present on the platinum metal particles and on the support. These materials exhibited some unique catalytic properties when compared to conventionally prepared platinum–tin bimetallic systems.

Since conventionally prepared materials almost invariably possess tin in an oxidized state (Sn^{2+}, Sn^{4+}), the novel feature of the SMAD approach is to obtain the Sn^0 state, and highly dispersed, small particles.

In spite of the commercial importance of Pt–Sn/support catalysts, which has inspired a great deal of work on these systems, the effect of tin on the platinum is still not well understood. In particular, the oxidation state of tin in the active catalyst is very difficult to ascertain (*6–10*).

Earlier studies suggested that zero-valent tin certainly has an effect on the platinum catalyst performance (*4, 5*). However, what might be more informative would be to study Pt–Sn bimetallic (both metals zero valent) catalysts. But how can such particles be prepared in a highly dispersed form? Thus we turned to the SMAD method again, where in this case both metals were evaporated simultaneously, the atoms solvated, and then allowed to deposit together on the catalyst support (the "full SMAD" method). This approach has been successful in earlier work with Co–Mn (*1b–d, 11*), Co–Fe (*12*), Fe–Mn (*12*), Pt–Re (*13*), and other combinations.

Herein, we report results on these full SMAD Pt–Sn/Al_2O_3 catalysts, including preparation, catalytic performance, and

0021-9517/90 $3.00

spectroscopic characterization (XRD, XPS, Mössbauer, and EXAFS).

EXPERIMENTAL

PREPARATION OF CATALYSTS

A. SMAD Catalysts

(1) Electron beam apparatus. An MK.5 Vapor Synthesizer (G. V. Planer Ltd, London) with two electron guns operating simultaneously was employed for Pt and Sn evaporation. About 5-g charges of the metals were placed on the copper hearths. These were melted and filament current increased to about 40 A. The emission current (about 200 mA) passed from the hot filaments to the metals and down through the water cooled hearths. During this time the vacuum was about 10^{-4} to 10^{-5} Torr. The vaporization chamber walls were cooled with liquid nitrogen. While the metals were evaporating, solvent (toluene or THF) was inletted as a vapor; about 220 ml of liquid was inletted over approximately 6 h. Usually about 1 g Pt and 0.8–1.5 g Sn were evaporated over this time, and the atoms solvated by the freezing solvent forming a frozen matrix. Upon completion of the deposition the matrix was allowed to warm to room temperature. During this period atom agglomeration took place so that solvated colloidal particles were formed. This resultant black solution was collected and poured over the pretreated Al_2O_3 support in an argon environment. Deposition/impregnation was allowed to proceed for 24 h (with stirring in order to obtain an even deposition/impregnation), after which solvent was evaporated leaving a black powder, which was homogeneous in appearance.

(2) Glass codeposition metal vapor apparatus (resistive heating). A simpler glass apparatus was also employed successfully, which has been described elsewhere (*1, 4, 5, 14*). However, one difference was that the glass reaction chamber possessed four copper electrodes instead of only two (see Fig. 1). One set of electrodes was equipped with a tungsten–Al_2O_3 coated crucible used for Sn evaporation. The other set of electrodes was equipped with a 4-in tungsten rod (1/8-in diameter) which was wrapped with Pt wire (1 in of 0.04-in diameter). The reaction chamber was pumped down to 10^{-4} Torr and cooled with liquid nitrogen. Solvent (toluene or THF) was inletted as a vapor while Pt (120 A current) and Sn (45 A current) were evaporated simultaneously. Over a 3-h period about 0.5 g Pt and 0.5–1 g Sn were codeposited with about 150 ml of solvent. A dark orange matrix was formed. Upon warming toward room temperature the color changed from orange to purple to blue, and finally to black (toluene). With THF, the matrix was initially yellow, then blue, and finally black. During these warming steps atom agglomeration to solvated colloidal particles took place.

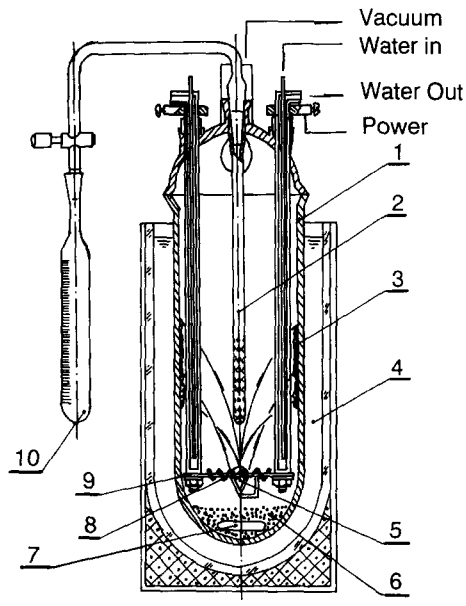

FIG. 1. A Full SMAD reactor. (1) reactor chamber; (2) solvent vapor inlet; (3) matrix; (4) liquid N_2; (5) vaporization crucible with Sn metal; (6) the calcined alumina; (7) magnetic stir bar; (8) Pt wire; (9) W rod; (10) Solvent.

The black liquid was allowed to flow down onto a pretreated Al_2O_3 catalyst support in

TABLE 1

Full SMAD Pt–Sn/Al_2O_3 Catalysts

Catalyst	Device	Solvent	Wt% Pt	Wt% Sn	Sn/Pt atomic ratio
A	Glass reactor	Toluene	0.62	1.01	2.7
B		Toluene	0.39	0.98	4.1
C		Toluene	0.04	0.96	39
D		Toluene	1.06	0.95	1.5
E		Toluene	0.37	1.92	8.5
F		THF	0.76	1.12	2.4
G	Electron beam	Toluene	0.92	1.50	2.7
H	Device	Toluene	0.94	0.91	1.6
I		Toluene	0.41	0.20	0.80

the bottom of the reaction chamber, impregnation took place over 24 h (with stirring in order to obtain an even deposition/impregnation), and the resultant slurry was siphoned out under argon. Solvent was removed leaving a black powder, which was homogeneous in appearance.

B. Conventional Catalysts

Two conventional catalysts were prepared and compared with the SMAD systems. One was prepared by coprecipitation (0.5% Pt and 1.0% Sn by weight on Al_2O_3) (*15*). Another was prepared by coimpregnation (0.5% Pt and 1.0% Sn by weight on Al_2O_3) (*16*).

Catalysts prepared are listed in Table 1. In all cases of the Al_2O_3 (γ-phase, 220 m^2/g) was pretreated by heating at 500°C with 200 ml/min flow of air followed by cooling under a flow of pure nitrogen. The SiO_2 (700 m^2/g) was pretreated in the same way. For full SMAD Pt—Sn/Al_2O_3 catalysts in Table 1, catalysts A–E and F were prepared in the glass apparatus, but samples A–E were prepared using toluene as solvent, while sample F was prepared with THF. Catalysts G–I were prepared using the electron beam apparatus (toluene as solvent). In this way, the effects of solvent and change in the apparatus used could be evaluated. In addition, with samples A–D, tin content was held constant (from 0.95 to 1.01 wt%), but Pt amounts varied. In this way, the effects of Pt loadings, when Sn loadings were fixed, could be examined. However, samples B, E, and I contained almost the same amounts of Pt (0.37–0.41 wt%), but the amounts of Sn in them were varied (from 0.2 to 1.92 wt%). In this way, the effects of Sn loadings in the catalysts could be examined, while Pt loadings were fixed.

XPS Experiments

The XPS data were acquired on a Leybold–Hereaus LHS-11 spectrometer. Catalyst samples were in powdered or extruded forms. The X-ray source (MgK = 1253.6 eV) was operated at 240 W. The vacuum during analyses was less than 1×10^{-7} Torr. Sample treatments were carried out in a high-temperature, high-pressure compartment attached to the side of the main analysis chamber. Transfer of the samples from this compartment to the analysis position was accomplished through a series of valveless and differentially pumped chambers without exposure to air. The fresh full SMAD Pt–Sn/Al_2O_3 catalyst samples were mounted on a palladium holder.

The Al_{2p} (74.7 eV) peak for the Al_2O_3 support was used for calibration of binding energies. Photoelectron lines for $Sn_{3d5/2}$, $Sn_{3d3/2}$, Cl_{2p}, Pt_{4f}, Al_{2p}, O_{1s}, and C_{1s} were recorded for all samples. Usually more than 50 scans were necessary to obtain good sig-

nal/noise ratios. Due to the extruded sample shapes and the fact that the powder samples were insulators, substantial charging effects could be expected. Thus we had to spend a great deal of time determining what these charging effects were, and correcting for them. Usually, the charging effects caused the binding energies to artificially increase. Therefore, we carefully determined the correct binding energy for the Al_{2p} band, and used this as a standard for correcting for charging effects.

For platinum XPS spectra, the position of the $Pt_{4f7/2}$ for metallic Pt was observed near 71.2 eV, while for Pt^{2+} and $Pt_{4f7/2}$ peak was near 73.0 eV. These are near the Al_{2p} peak (74.7 eV) which caused some difficulty in clearly resolving the peaks due to Pt in the catalysts. Therefore, we attempted to deconvolute the XPS data obtained under high resolution by using doublets for the $Sn_{3d5/2}$ and $Sn_{3d3/2}$ peaks and for the $Pt_{4f7/2}$ and $Pt_{4f5/2}$ peaks. This allowed better separation of peaks for tin on the palladium holder, platinum peaks, and aluminum peaks.

Mössbauer Experiments

A computerized MS-1200 Mössbauer Spectrometer (Ranger Scientific) was used for collecting Mössbauer spectra. The instrument was operated in an acceleration mode. A 10-m Ci $^{119}CaSnO_3$ source was used for ^{119}Sn Mössbauer measurements. A velocity range from -6 to $+6$ mm/sec was used, which was calibrated by a laser device in the transducer. In order to rule out the effects of X rays, produced by the source, a piece of palladium foil of 0.05 mm thickness was placed in front of the sample being analyzed. Catalyst samples (450 mg) were sealed in a holder under argon and then mounted in the spectrometer.

EXAFS Experiments

X-ray absorption spectra were recorded at the Cornell High Energy Synchroton Source (CHESS) facility in the fluorescence mode for tin. Reference materials were tin metal foil, $SnCl_4$, $SnCl_2$, SnO, SnO_2, and a bulk Pt–Sn 1 : 1 alloy (collected at the *K*-edge at 29.19 KeV). All the spectra were reduced using computer codes developed at Cornell, which provided for successive refinement of the radial distribution functions (RDFs) (*17, 18*). One to three scans were recorded for each sample. Initially the entire spectrum (to $K = 16$ Å^{-1}) was reduced even when there was a great deal of noise at high K, in order to achieve the best resolution in the RDF curves.

XRD Experiments

A XDS-2000 Spectrometer using Cu$K\alpha$ radiation (Scintag, Inc.) was employed for powder X-ray diffraction studies. The tube voltage was 40 kV, current was 45 mA, and the scanning rate was 2.5°/min. Every sample was carefully ground and fully packed into the XRD sample cell.

Catalyst Testing

Catalyst performance was determined using a microreactor-GC system pulse flow system, which has been described elsewhere (*4*). The feed stock was *n*-heptane. The rate of hydrogen flow at 1 atm was 140 ml/min, and 0.2 g of catalyst sample was placed in a reactor with 6 mm in diameter. Each injection of 1 μl of *n*-heptane was carried by the hydrogen flow and passed through a preheating tube, then, to the catalyst bed. The *n*-heptane pulse contacted the catalyst bed for a very short time, and this contact time depended on the hydrogen flow rate. The products went directly to an online GC for analysis. After the injection, only pure hydrogen passed through the catalyst bed. The conversion data reported herein were repeated at least three times, before changing to other conditions or experiments.

RESULTS

XPS Data

Typical tin XPS data (for catalyst G) are shown in Fig. 2. The peak positions have been corrected for sample charging by using the Al_{2p} peak as a standard at 74.7 eV. Note

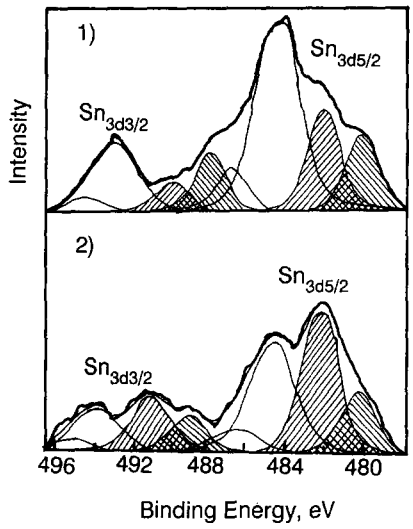

FIG. 2. The XPS spectra for catalyst G and the substraction of charging peaks from the spectra: (1) fresh catalyst; (2) after oxidation *in situ* at 400°C.

that the shaded peaks are in lower binding energy positions compared with the position for metallic Sn (484.7 eV) in the catalyst samples. Obviously, it is not possible that there are any Sn species on the catalysts whose binding energies are lower than that of Sn metal. So, we conclude that the shaded peaks represent species which do not experience charging. In other words, these low binding energy species are not in the samples but are instead from the Pd holder in our system. During sample treatments (for example, pumping down, doing *in situ* oxidation or reduction, etc.), some Sn was shifted to the Pd holder, and this Sn did not experience a charging effect because the Pd holder is a good conductor and was well grounded. Corrections for charging effects and these anomalous peaks have been made. Therefore, the shaded peaks in Fig. 2 are not considered in the following discussion.

The spectra for the Al_{2p} and Pt_{4f} regions are shown in Fig. 3 for catalyst E. The deconvolution was carefully carried out assuming the intensity ratio of $4f5/2 : 4f7/2$ to be 0.75 : 1.0. The XPS data are summarized in Table 2.

Mössbauer Data

The ^{119}Sn Mössbauer spectra for standard samples are shown in Fig. 4, and their parameters are listed in Table 3. There are significant differences in the isomer shifts (IS) for Sn metal vs PtSn alloy vs SnO_2 and $SnCl_2$. Quadrupule splitting (QS) and peak width at half maximum (PWHM) are different for SnO_2 vs $SnCl_4$. Based on the data for the standards and spectral fitting for the SMAD catalysts, the Mössbauer parameters for the catalysts are listed in Table 4, and the spectra are shown in Fig. 5. Generally the full SMAD catalysts prepared by the electron beam method or the resistive heating method using either toluene or THF as solvents showed the same Mössbauer parameters. However, with high tin loadings a Mössbauer peak due to Sn^{4+} was observed in addition to the peak for Sn^0. This was especially evident for catalyst F which was prepared using THF, which suggests that some tin oxidation was caused by THF during the atom/clustering process.

EXAFS Data

The peaks in the radial distribution functions for catalysts G and H (for the Sn *K*-

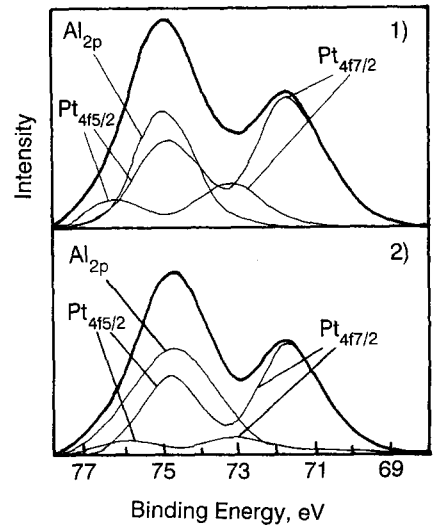

FIG. 3. The XPS spectra of Pt_{4f} for catalyst E: (1) oxidized catalyst; and (2) fresh catalyst.

TABLE 2

XPS Parameters for Full SMAD Pt–Sn/Al_2O_3 Catalysts

Catalyst[a]	State	Binding energy eV	Relative area, %	Species assigned
A		484.7	89.2	Sn(O)
	Fresh	486.1	10.8	Sn(II) & Sn(IV)
		71.5	100.0	Pt(O)
		484.2	86.2	Sn(O)
	Oxidized	486.0	13.8	Sn(II) & Sn(IV)
		71.1	100.0	Pt(O)
B		484.7	84.1	Sn(O)
	Fresh	486.8	15.9	Sn(II) & Sn(IV)
		71.4	100.0	Pt(O)
		484.9	80.9	Sn(O)
	Oxidized	486.8	19.1	Sn(II) & Sn(IV)
		71.9	100.0	Pt(O)
G		484.9	88.1	Sn(O)
	Fresh	486.6	11.9	Sn(II) & Sn(IV)
		71.8	100.0	Pt(O)
		484.8	88.7	Sn(O)
	Oxidized	486.4	11.3	Sn(II) & Sn(IV)
		71.3	100.0	Pt(O)
H		484.0	84.9	Sn(O)
	Fresh	486.0	15.1	Sn(II) & Sn(IV)
		71.3	90.8	Pt(O)
		73.2	9.2	PtO
		484.4	53.0	Sn(O)
	Oxidized	486.0	47.0	Sn(II) & Sn(IV)
		71.6	76.4	Pt(O)
		73.0	23.6	PtO

[a] Catalysts A and B were prepared in glass apparatus; catalysts G and H in electron beam apparatus.

edge spectra) are shown in Fig. 6. Assignments of the catalyst's RDFs are based on reference compound spectra (*19*). For clarity, the reduced radial distribution peaks at Sn *K*-edge for the reference compounds and catalysts G and H are summarized as follows:

Material	Peak position (Å)			
$SnCl_4 \cdot 5H_2O$	2.26(295)			
$SnCl_2 \cdot 2H_2O$	2.16(40)	2.59(101)	3.33(45)	4.50(63)
SnO_2	2.05(276)		3.19(277)	3.71(665)
SnO	2.18(114)			3.48(373)
Sn metal			2.82(88)	
Sn–Pt alloy			2.83(220)	3.96(90)
Full SMAD catalyst G	2.26(60)		2.86(610)	3.48(90)
Full SMAD catalyst H	2.16(45)		2.84(680)	3.54(88)

The area of the peaks are given in parentheses. Note the similarities of the spectral features of the SMAD catalysts compared with the Sn–Pt alloy.

XANES features at Sn *K*-edge for reference compounds and the SMAD catalysts G and H were also obtained by determination of the edge positions. All edge positions were determined (see following data) from the energy derivative curves, and were measured relative to those of Sn metal, assigned zero.

Material (at Sn *K*-edge)	E_0 (eV)
Sn metal	(0)
Sn–Pt alloy	−1–+2
$SnCl_2 \cdot 2H_2O$	−0.6–0
SnO	0.5
$SnCl_4 \cdot 5H_2O$	4
SnO_2	5
Full SMAD catalyst G	−1–0
Full SMAD catalyst H	−1–0

From the XANES data, it can be seen that the edge position has a feature of positive

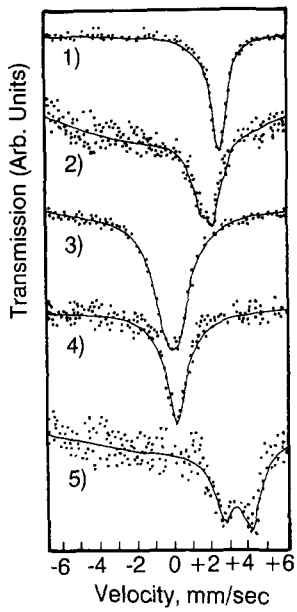

FIG. 4. The ^{119}Sn Mössbauer spectra for some standards (at room temperature): (1) Sn metal; (2) PtSn alloy; (3) SnO_2; (4) $SnCl_4$; (5) $SnCl_2$.

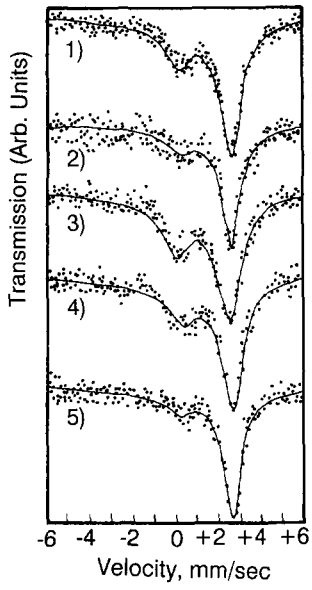

FIG. 5. The ^{119}Sn Mössbauer spectra at room temperature for: (1) catalyst A; (2) catalyst B; (3) catalyst F; (4) catalyst G; (5) catalyst H.

displacement with oxidation number. Unfortunately, there is not a clear-cut differentiation among $SnCl_2 \cdot 2H_2O$, Sn–Pt alloy, and Sn metal. However, it is clear that the Sn in catalysts G and H could not be mainly present in the form of SnO_2, $SnCl_4 \cdot 5H_2O$, or SnO. Moreover, the main peaks of catalysts G and H were similar to those found for the Sn–Pt alloy, not to $SnCl_2 \cdot 2H_2O$. Also, by considering other data, such as how the sample was prepared, as well as Mössbauer (discussed later), the presence of $SnCl_2 \cdot 2H_2O$ can be ruled out. Therefore, the combined evidence supports the presence of Sn–Pt-alloy-like particles in these SMAD catalysts.

TABLE 3

Mössbauer Parameters for Some Standards

Sample	IS[a] mm/sec	QS mm/sec	Linewidth mm/sec
Sn metal	2.55	0.00	0.57
PtSn alloy	1.84	0.68	0.59
$SnCl_4$	0.16	0.11	0.62
SnO_2	0.03	0.73	0.81
$SnCl_2$	3.41	1.40	0.61

[a] IS with respect to $CaSnO_3$.

X-Ray Diffraction (XRD) Data

X-ray diffraction data for full SMAD catalyst A, and conventionally prepared Pt–Sn/Al_2O_3, coimpregnated Pt–Sn/Al_2O_3, and Al_2O_3 (γ form in all cases) are shown in Fig. 7. Bar lines in Fig. 7 show known XRD patterns for a standard Pt_3Sn alloy, γ–Al_2O_3, and Pt metal. It can be seen that the peak intensities at 2θ = 25–45° for the coimpregnated catalyst are higher than those for the coprecipitated one. For both of them, however, intensities are higher than for the full SMAD catalyst; in fact the spectrum for the SMAD catalyst is the same as that for γ–Al_2O_3. This means that metal particle sizes in the full SMAD catalyst are extremely small and/or amorphous.

Catalyst Testing Data

The effects of solvents and apparatus. Samples A and F were prepared by the full

TABLE 4

Mössbauer Parameters for Various Full SMAD Pt–Sn/Al_2O_3 Catalysts

Sample[a]	IS mm/sec	QS mm/sec	Linewidth mm/sec	Relative area, %	Species assigned
	0.06	0.13	0.67	25	Sn(IV) oxides
Catalyst A	1.82	0.63	0.58	7	PtSn alloy
	2.55	0	0.55	68	Sn(O)
	0.04	0.18	0.64	17	Sn(IV) oxides
Catalyst B	1.86	0.63	0.55	8	PtSn alloy
	2.53	0	0.54	75	Sn(O)
	0.05	0.20	0.67	31	Sn(IV) oxides
Catalyst F	1.84	0.63	0.55	15	PtSn alloy
	2.51	0	0.55	54	Sn(O)
	0.19	0.28	0.67	26	Sn(IV) oxides
Catalyst G	1.84	0.58	0.58	8	PtSn alloy
	2.55	0	0.55	66	Sn(O)
	0.09	0.08	0.63	13	Sn(IV) oxides
Catalyst H	1.95	0.60	0.60	5	PtSn alloy
	2.55	0	0.55	82	Sn(O)

[a] Catalysts A and B were prepared by using toluene solvent in glass apparatus; catalyst F was prepared by using THF solvent in glass apparatus; catalysts G and H were prepared by using toluene solvent, but in electron beam apparatus.

SMAD process in the same glass apparatus, but using different solvents (toluene for sample A and THF for sample F). The yield of aromatics (toluene and benzene from *n*-heptane) produced by both catalysts were almost the same; 64.5 and 64.8 wt%, respectively (see Table 5). The cracking products (C_1–C_6) and their distributions are essentially identical.

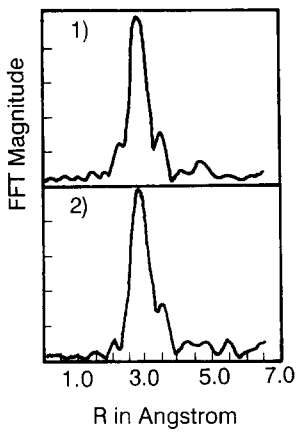

FIG. 6. EXAFS-RDFs for: (1) catalyst G; and (2) catalyst H (uncorrected phase shift, at Sn K-edge).

Catalysts D and H contained nearly the same amounts of Pt and Sn (Table 5) and were prepared using the same solvent (toluene), but in a different apparatus (in the glass apparatus for catalyst D and in the electron beam apparatus for catalyst H). It can be seen from Table 5 that the aromatics are 64.5 and 63.4 wt%, and C_1–C_6 products are 35.5 and 35.4 wt%, respectively.

Therefore, we conclude that, under our conditions, the two solvents and apparatus we used for the full SMAD procedure did not affect the catalytic performance of the catalysts obtained.

The effects of Pt loadings in the catalysts. In the full SMAD samples A–D (Table 1 and 5), there were very similar loadings of Sn (0.95–1.01 wt%), but the amounts of Pt varied from 0.04–1.06 wt%. Based on such samples (the amounts of Sn in the catalysts were fixed), the catalytic testing data were

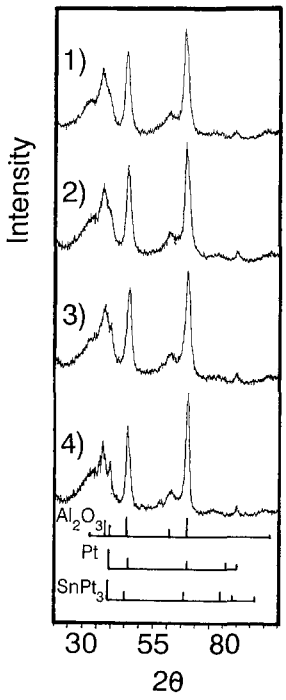

FIG. 7. XRD spectra for: (1) Al_2O_3; (2) Full SMAD catalyst A; (3) Coprecipitated Pt–Sn/Al_2O_3 catalyst (0.5 wt% Pt; 1.0 wt% Sn); (4) Coimpregnated Pt–Sn/Al_2O_3 catalyst (0.5 wt% Pt; 1.0 wt% Sn).

compared in order to observe the effects of Pt loadings in the catalysts.

Thus, the yields of aromatics (toluene and benzene) from *n*-heptane passing over the

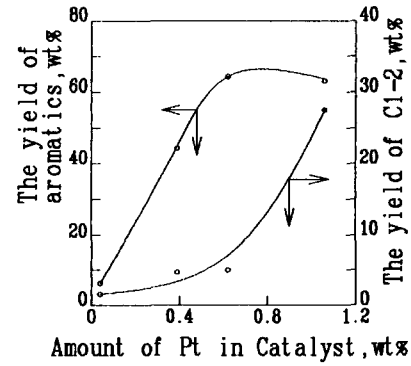

FIG. 8. Dehydrocyclization and hydrogenolysis vs amount of Pt in catalysts A, B, C, and D (the amounts of Sn in the catalysts are 0.96–1.01 wt%; see Table 1).

full SMAD catalysts are listed in Table 5. In Fig. 8 the yields of aromatics and C_1–C_2 products are compared with the Pt loadings. When the Pt content is over 0.62% the yield curve for aromatics flattens out while C_1–C_2 product yields increase significantly. Catalyst A (loadings of Pt = 0.62 wt% and Sn = 1.01 wt%) exhibits the best catalytic properties with high aromatics yield and low C_1–C_2 yields. In other words, the aromatization ability of the catalyst decreases when the Pt loading is less than 0.62 wt%. When the loading of Pt is over 0.62 wt%, the aromatization ability does not increase, but hydrogenolysis products C_{1-2} do significantly in-

TABLE 5

The Distribution of Products from *n*-Heptane on Various Full SMAD Catalysts (at 500°C)

Catalyst	Loading of metal, wt%[a]		C_{1-2}	C_{3-4}	C_{5-6}	B[b]	iC_7	nC_7	T
	Pt	Sn							
A	0.62	1.01	4.9	10.6	11.4	16.3	6.6	2.0	48.2
B	0.39	0.98	4.1	5.2	9.6	4.4	13.9	24.0	38.8
C	0.04	0.96	1.3	1.7	1.4	1.4	4.6	85.6	4.0
D	1.06	0.95	25.7	9.0	1.5	29.9	0	0	33.9
E	0.37	1.92	—	—	11.3	0.3	30.4	51.7	6.3
F	0.76	1.12	5.1	11.1	10.7	15.9	7.1	1.2	48.9
G	0.92	1.50	2.0	2.7	17.2	3.0	18.3	31.3	25.5
H	0.94	0.91	24.1	10.0	1.3	27.8	1.2	0	35.6
I	0.41	0.20	11.2	10.1	10.6	4.2	10.2	13.5	40.2

[a] For atomic Sn/Pt ratios, see Table 1.
[b] B = Benzene, and T = Toluene.

crease, which is not desirable. Therefore, our results suggest that Pt is necessary to promote aromatization, but also cracking and hydrogenolysis. On the other hand, the presence of Sn seems to inhibit cracking and hydrogenolysis.

The effects of Sn loadings in the catalysts. Among the samples we prepared in this study, catalysts B, E, and I contain very similar amounts of Pt (0.37–0.41 wt%). However, the loadings of Sn varied from 0.20, 0.98 to 1.92 wt%. It can be seen from data in Table 5 that when the loading of Sn is too high, for example in catalyst E, catalytic processes were severely inhibited. When the loading of Sn was lower, for example in catalyst I, catalytic properties were similar to that of Pt/Al_2O_3 alone, showing high cracking ability (catalytic data for Pt/Al_2O_3 were reported earlier (*4*). Only when the Pt and Sn loadings are high enough and when the ratio of Sn/Pt is in an appropriate range does a synergistic effect become important. For example, catalysts A and F have atomic ratios of Sn/Pt = 2.7 and 2.4, respectively, and both possess very good catalytic properties with high conversions, high yields of aromatics, and low yields of C_{1-2}. Thus, both loading level and Sn/Pt ratios are important, and under our experimental conditions the best Sn/Pt ratio appears to be about 2.5/1.

Comparisons with conventionally prepared catalysts were also carried out, using samples with similar loadings of Pt and Sn. Figure 9 illustrates the yields of aromatics and C_{1-2} vs reaction temperature for full SMAD catalyst A, a conventionally prepared coprecipitated $Pt–Sn/Al_2O_3$ catalyst (0.5 wt% Pt and 1.0 wt% Sn), and a half SMAD catalyst (0.6 wt% Pt and 1.0 wt% Sn) (*4*). It is clear from the plot that catalyst A allowed the highest yield of aromatics along with the lowest yield of C_{1-2} hydrogenolysis products, with a reaction temperature of 500°C.

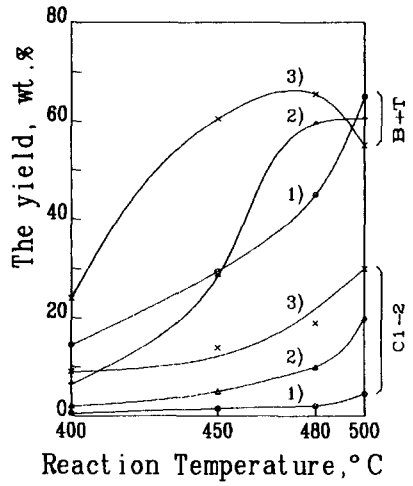

FIG. 9. The yields of benzene and toluene (B + T), and C_{1-2} vs Reaction temperature for (1) full SMAD $Pt–Sn/Al_2O_3$ catalyst A; (2) coprecipitated $Pt–Sn/Al_2O_3$ catalyst (0.5 wt% Pt; 1.0 wt% Sn); (3) half SMAD $Pt–Sn/Al_2O_3$ catalyst (0.6 wt% Pt, 1.0 wt% Sn).

DISCUSSION

From the XRD experiments (see Fig. 7) we found that SMAD, Pt, and Sn particles on Al_2O_3 were either very small and/or amorphous, which was in contrast to the conventionally prepared catalysts. The next question deals with whether the Pt–Sn particles are atomically mixed or separate metallic Pt and Sn particles. When XPS was utilized, we found that Sn_{3d} peaks for a bulk Pt–Sn alloy did not exhibit a noticeable shift compared with a Sn metal film. However, we did find that for the full SMAD $Pt–Sn/Al_2O_3$ catalyst, Sn^0 was the main component, usually more than 84% of total tin detected (as Sn^0, Sn^{2+}, and Sn^{4+}). Even after vigorous oxidation treatments Sn^0 remained (Table 2). Pt^0 also dominated over Pt^{2+}, as expected, even after oxidation treatments. Our previous results with half SMAD $Pt–Sn/Al_2O_3$ (Sn deposited on preformed Pt particles) and conventional $Pt–Sn/Al_2O_3$ catalysts always showed a sensitivity of Sn^0 toward oxidation (*4*, *5*). In fact in conventional preparations the tin is generally all in the form of Sn^{2+} and Sn^{4+}. So the full SMAD Pt–Sn particles are very unusual in their oxidative stability. We believe this behavior (a very high resistance to oxidation of Sn^0 or Pt^0) is due to the formation of

atomically mixed Pt–Sn metallic particles, which greatly inhibits oxidation of the Sn^0 in the intimate particles. In other words, our XPS results provide strong, although indirect, evidence of the presence of Pt–Sn bimetallic particles.

In addition, there is direct evidence for such Pt–Sn mixed particles. In the tin Mössbauer a doublet peak with IS = 1.82–1.95 mm/sec with QS = 0.58–0.63 mm/sec (Table 4 and Fig. 5) strongly supports the presence of Pt–Sn bimetallic particles. Also, EXAFS data (Fig. 6) strongly suggests the presence of such particles.

From these data (XPS, Mössbauer, and EXAFS) we conclude that Pt–Sn bimetallic particles are prevalent on the full SMAD catalysts.

Is it also possible to say something about the structure of these bimetallic particles, based on our spectral data? We note from Tables 2 and 4 that there are differences in the relative amounts of the various species detected. For example, the XPS data (Table 2) for fresh full SMAD catalysts, Sn^0 accounts for 84–89% of the total tin, while Pt^0 accounts for 91–100% of the total platinum detected. On the other hand, the Mössbauer data (Table 4) for the same catalysts A, B, G, and H, only 5–8% of the Sn^0 is in the form of Pt–Sn bimetallic particles, with much larger amounts (66–82%) of tin as Sn^0 not associated with Pt–Sn particles. We note that XPS is a surface analysis technique, and Mössbauer a bulk analysis technique. The XPS detection of Sn^0/Pt^0 ratios of near 1 : 1, while Mössbauer detects much larger amounts of Sn^0 not associated with Pt^0, could be explained by two scenarios. First, most of the Pt^0 and Sn^0 deposit as individual Pt and Sn particles along with smaller individual Pt–Sn metallic particles. Second, most of the Pt and Sn deposit together but as partially segregated phases with a small amount of Pt–Sn bimetallic phase on the top. Since the first scenario might be predicted to not yield catalytically altered properties (individual platinum particles exist without the benefit of tin alteration), and since catalytic properties are indeed altered by tin, we favor the second scenario (Fig 11).

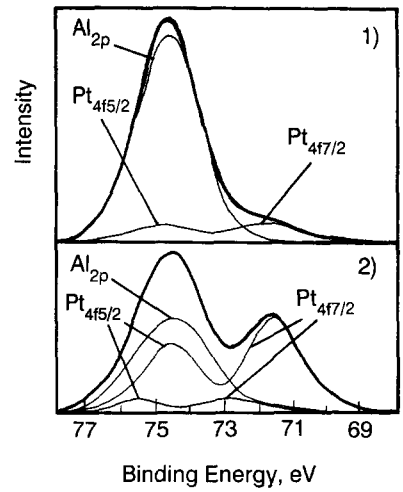

FIG. 10. The comparison of XPS Pt_{4f} peaks for: (1) catalyst E; and (2) catalyst B.

We noticed another interesting effect when tin loadings were very high (that is, the Sn/Pt ratio was high). The ratio of Pt/Al in the catalysts has been compared by looking at the XPS Pt_{4f} and Al_{2p} peak areas. For catalyst E the XPS data showed a Pt : Al ratio of 1 : 10; for catalyst B a 8.4 : 10 ratio (see Fig. 10). For both these catalysts the Pt loadings were about the same, but the Sn loadings varied (B, 0.98 and E, 1.9). In other words, the surface Pt detected was much higher when Sn loading was lower. Also, we note that the catalyst with the very high tin loading (catalyst E) had poorer catalytic behavior (Table 5). These results suggest that too much tin can cover up Pt and Sn–Pt particles, and thereby hurt catalytic properties.

Further evidence about particle structure can be gleaned from the EXAFS data. Both Pt–Sn bonds and Sn–O bonds were detected. Since solvated Sn atoms would be susceptible to oxidation by surface –OH groups on the Al_2O_3 surface, as we have found for Mn, Fe, and Co systems (*1, 11, 12*) we believe that initial nucleation of tin and Pt–Sn particles may occur when a solvated Sn atom is attached by a surface –OH

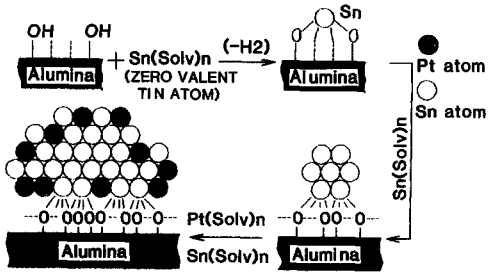

FIG. 11. Proposed beginning sequence for formation of full SMAD Pt–Sn bimetallic particles on Al_2O_3. A Sn/Pt atomic ratio of 2.5 is illustrated, such as that for catalyst A.

group. We have encountered this behavior with several other metals (*1, 11, 12*) as have Ozin and co-workers (*2*).

Considering all this spectroscopic evidence, we believe the best working model for the full SMAD Pt–Sn/Al_2O_3 is with a tin-oxide underlayer formed when solvated Sn atoms react with surface –OH groups (Fig. 11). This site then serves as a nucleation site for further Sn atoms and Pt atoms. If too much tin is available, some Pt can be covered and/or diluted too much:

The oxidative properties of the Pt–Sn bimetallic phase is quite remarkable. For example catalyst H was exposed to air at room temperature for 1 week and then for 6 months (Fig. 12). Mössbauer analysis clearly showed the slow growth of tin oxides and decrease in Sn^0. However, we call attention to the region where tin absorbs in the Pt–Sn bimetallic particles (IS = 1.86 mm/sec). Computer fitting shows that Sn^0 greatly decreases (40 → 10% of total), but the tin absorption for Pt–Sn does not change. This was true for several full SMAD catalysts after extended periods of exposure to oxygen. These results show that the Pt–Sn particles are remarkably oxidation resistant.

Catalytic Performance

As mentioned above, the full SMAD procedure results in the formation of some Pt–Sn bimetallic phase. However, catalytic testing data show that it is not true that all full SMAD catalysts with different Pt and Sn loadings yield good catalytic results. When the loading of Sn was about 0.95–1.01 wt%, activity was not good for the catalysts with less than 0.62 wt% of Pt, and selectivity was poor for catalysts with more than 0.62 wt% of Pt.

Moreover, if there are relatively low loadings of Pt (0.37–0.41 wt% in the present study), with high loadings of Sn, such catalysts exhibit poor activity, and lower loadings of Sn did not improve the properties. Therefore, suitable amounts of Pt and Sn in the full SMAD catalysts are very important. For our case, the best composition for a full SMAD catalyst was 0.62 wt% of Pt and 1.01 wt% of Sn (catalyst A).

In conventional Pt–Sn/Al_2O_3 catalysts prepared by the coprecipitation method, the Sn component interacts with the alumina support to form a $SnO_2 \cdot Al_2O_3$ ($SnAl_2O_5$) structure, which improves the properties of support, leading to better stability and a lower rate of coke formation (*8, 20*).

The fact that three different particle models are obviously important when considering the three different preparation techniques (conventional, half SMAD (*4, 5*) and

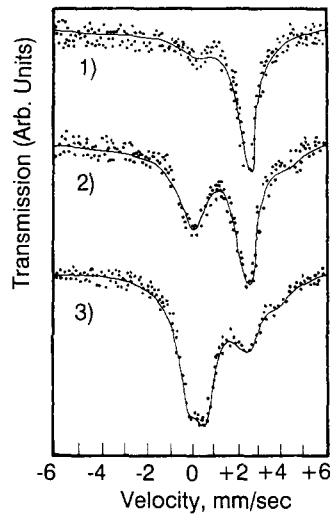

FIG. 12. The ^{119}Sn Mössbauer spectra at room temperature for: (1) fresh catalyst H; (2) exposed to air for 1 week; (3) exposed to air for 6 months.

TABLE 6

Summary of Various Pt–Sn/Al_2O_3 Catalysts[a]

Preparation method	Oxidation state of Sn	Proposed morphology	Conversion of *n*-heptane*
Coprecipitation	Sn(IV) oxides	SnO_2 interacted with support Al_2O_3 to prevent Pt particles growing very large	Stability: significantly improved Selectivity: better to aromatics Activity: small decrease
Half SMAD method	Sn(O) metal with carbonaceous species	Sn(O) metal and Pt(O) metal are dispersed on Al_2O_3 and some Pt(O) clusters are partially covered by Sn(O) atoms	Stability: the same or a little improvement Selectivity: the same or a little improvement Activity: increased
Full SMAD	Sn(O) alloys with Pt(O)	Sn^{4+} and Sn^0 base is surrounded by a PtSn alloy	Stability: the same Selectivity: greatly depressed hydrogenolysis Activity: small decrease

[a] Compared with Pt/Al_2O_3 catalyst.

full SMAD), suggests that catalyst testing on all three under the same conditions could yield valuable information. Therefore, we have carried out such studies.

From catalytic testing data, the full SMAD catalysts appear to be unique compared with the half SMAD (*4, 5*) and conventional catalysts. The data in Table 5 and Figs. 8 and 9 suggest that, because of the presence of Pt–Sn bimetallic particles, hydrogenolysis is significantly depressed. Only when relatively high loadings of Pt were used, such as in catalyst D, did hydrogenolysis products C_1 and C_2 increase to values characteristic for Pt/Al_2O_3 catalysts (SMAD or conventional). These results suggest that platinum alone plays the most important role in unwanted hydrogenolysis. We also noted, however, that the desired dehydrocyclization ability of the catalysts was not significantly different for the full SMAD Pt–Sn/Al_2O_3 systems compared with other systems. So the full SMAD catalysts possessed good dehydrocyclization ability, while depressing unwanted hydrogenolysis (Fig. 9). It is tempting to attribute this behavior to an ensemble effect where the structure sensitive hydrogenolysis reactions are discouraged because of the presence of some Sn^0 atoms on/in the surface of the Pt particle.

One interesting facet of this work and our earlier work with half SMAD Pt–Sn catalysts should not be overlooked; that is that the presence of Sn^0 does have significant catalytic effects on the Pt. Our results, overall, lend support to the idea that zero-valent tin, although rarely spectroscopically detected in conventional Pt–Sn catalysts, may be the important chemical state that causes such beneficial changes in this very important class of reforming catalysts.

Considering all of our previous work on conventional (*6–10, 20*) half SMAD (*4, 5*) and now, full SMAD Pt–Sn catalysts, we can now make some useful generalizations, which are summarized in Table 6. We suggest that: (1) for conventional coprecipitated

systems, tin oxides present can improve the lifetime/stability of the catalyst, perhaps by blocking Pt particle sintering; (2) the presence of small amounts of Sn^0 on the surface of the Pt particles, can cause an increase in catalytic activity, especially at lower-reaction temperatures (such as in our half SMAD system) (*4, 5*); and (3) the presence of Pt–Sn bimetallic particles can significantly depress hydrogenolysis while still maintaining good activity for dehydrocyclization.

We believe, therefore, that control of tin oxidation states and particle size/morphology is possible by using different preparation methods as described herein, and catalytic properties can be predictably modified.

ACKNOWLEDGMENTS

We thank Dr. B. H. Davis (Center for Applied Energy Research) and Dr. S. H. Bauer (Cornell University) for use of XPS equipment and the Synchrotron device for EXAFS experiments and for helpful advice and discussions. The support of the National Science Foundation is acknowledged with gratitude.

REFERENCES

1. (a) Klabunde, K. J., and Tanaka, Y., *J. Mol. Catal.* **21,** 57 (1983); (b) Imizu, Y., and Klabunde, K.J., *in* "Catalysis of Organic Reactions" (R. Augustine, Ed.), p. 225. Dekker, New York, 1985; (c) Klabunde, K. J., and Imizu, Y., *J. Amer. Chem. Soc.* **106,** 2721 (1984); (d) Tan, B. J., Klabunde, K. J., Tanaka, T., Kanai, H., and Yoshida, S., *J. Amer. Chem. Soc.* **110,** 5951 (1988).
2. Ozin and co-workers are also using the solvated metal atom approach to prepare interesting catalytic materials; Woo, S. J., Godber, J., and Ozin, G. A., *J. Mol. Catal.* **52,** 241 (1989).
3. Klabunde, K. J., Jeong, G. H., and Olsen, A. W., *in* "Molecular Structure and Energetics" (J. E. Liebman and A. Greenberg, Ed.). VCH publishers, New York, **12,** 433 (1990).
4. Li, Yong-Xi, and Klabunde, K. J., *Langmuir* **3,** 558 (1987).
5. Li, Yong-Xi, Zhang, Yong-Fu, and Klabunde, K.J., *Langmuir* **4,** 385 (1988).
6. Dautzenberg, F. M., Helle, J. N., Biloen, P., and Sachtler, W. M. H., *J. Catal.* **63,** 384 (1980).
7. Bacaud, R., Bussiere, P., and Figueras, F., *J. Catal.* **69,** 399 (1981).
8. (a) Völter, J., Lieske, H., and Lietz, G., *React. Kinet. Catal. Lett.* **16,** 87 (1981); (b) Völter, J., Lietz, G., Uhlemenn, M., and Hermann, M., *J. Catal.* **68,** 42 (1981); (c) Lietz, G., Völter, J., Dobrovolszky, M., and Paal, Z., *Appl. Catal.* **13,** 77 (1984).
9. Burch, R. J., *J. Catal.* **71,** 348, 360 (1981).
10. Sexton, B. A., Hughes, A. E., and Foger, K., *J. Catal.* **88,** 466 (1984).
11. Tan, B. J., Klabunde, K. J., and Sherwood, P. M. A., submitted for publication.
12. Tan, B. J., Klabunde, K. J., and Sherwood, P. M. A., *Chem. Mater.*, **2,** 186 (1990).
13. Ahkmedov, V., and Klabunde, K. J., *J. Mol. Catal.* **45,** 193 (1988).
14. Klabunde, K. J., Timms, P. L., Skell, P. S., and Ittel, S., *Inorg. Syn.* **19,** 59 (1979).
15. Li, Yong-Xi, and Shia, Yuan-Fu, *Hyperfine Interact.* **28,** 875, 879 (1986).
16. Li, Yong-Xi, and Shia, Yuan-Fu, *in* "Proceedings of International Conference on the Applications of the Mössbauer Effect (Jaipur), 1982," p. 438.
17. Chiu, N. S., Bauer, S. H., and Johnson, M. P. L., *J. Catal.* **98,** 32 (1986).
18. Chiu, N. S., Bauer, S. H., and Johnson, M. P. L., *J. Catal.* **89,** 226 (1984).
19. Li, Yong-Xi, Chiu, N. S., Lee, W. H., Bauer, S. H., and Davis, B. H., *ACS Symp Ser* **411,** 328 (1989).
20. Li, Yong-Xi, and Shia, Yuan-Fu., "Oil and Gas in China," Vol. 1, p. 161, 1985.